



Three-body dissociation dynamics of $(\text{SO}_2)_3$ studied through dissociative photodetachment of $(\text{SO}_2)_3^-$

Todd G. Clements, A.K. Luong, Robert E. Continetti *

Department of Chemistry and Biochemistry, University of California, San Diego, 9500 Gilman Drive, La Jolla, CA 92093-0340, USA

Received 21 June 2002; in final form 4 October 2002

Abstract

The dissociative photodetachment dynamics of $(\text{SO}_2)_3^-$ were studied by photoelectron–photofragment coincidence spectroscopy at 258 nm. Correlation between the photoelectron and photofragment translational energies was observed as previously seen in the dimer system, implying the presence of a dimer core. The three-body dissociation dynamics of $(\text{SO}_2)_3$ after photodetachment are consistent with a dimer core solvated by a spectator SO_2 molecule with a broad distribution in initial geometry.

© 2002 Elsevier Science B.V. All rights reserved.

1. Introduction

The study of small molecular clusters can be used to provide insight into bulk dynamics [1] as well as detailed information on molecular interactions. As cluster size increases, the properties of the cluster tend towards those of the bulk. However, bulk dynamics are ultimately dependent on the interactions of smaller groups of molecules within the cluster making a detailed understanding of the dynamics of small clusters critical. For atmospherically important systems such as SO_2 , both the microscopic and macroscopic properties are of interest and can be probed through study of SO_2 clusters.

The photodestruction dynamics of anionic clusters of SO_2 have been studied by a number of

laboratories [2–8]. Specifically, elucidating the bond structure between the SO_2 moieties in $(\text{SO}_2)_2^-$ has been a common goal. Berthe-Gaujac et al. [9,10] studied $(\text{SO}_2)_2^-$ via ab initio methods and located several minima corresponding to S–S and S–O bond formation, consistent with the suggestion by Iraqi et al. [11] that variations in ion source conditions can result in creation of different isomers. Kim and Bowers [8] performed photodissociation studies of the dimer anion and showed evidence for the O–O bound dimer using an impulsive model of the ionic photodissociation dynamics. Based on photoelectron spectroscopy, Tsukuda et al. [4] propose an S–S bound dimer as most consistent with the data. Continetti and co-workers [3] studied energy partitioning over a wide range of energies using photoelectron–photofragment coincidence (PPC) spectroscopy and found evidence for an S–O bound dimer within the impulsive model. The wide range of results illustrates

* Corresponding author. Fax: +1-858-534-7244.

E-mail address: rcontinetti@ucsd.edu (R.E. Continetti).

the difficulty inherent in studying complex many-body systems.

For larger clusters, the progression in the photoelectron spectra for clusters of between three and six SO₂ molecules suggest that the dimer core remains present, and further SO₂ molecules simply solvate the core by about 0.3–0.4 eV each [4]. Photodissociation studies by Weber and co-workers [5] also indicate the presence of a dimer anion core surrounded by neutral molecular SO₂. While there is ample evidence for the presence of an anionic dimer core, little is known about the dissociation dynamics of these clusters.

PPC spectroscopy has been shown to be a useful method for studying the energetics and dynamics of small clusters [12]. For (SO₂)₃⁻, PPC spectroscopy will be used to study the dissociation dynamics of the photodetached neutral, and gain insight into the structure of the parent anion. In agreement with previous studies, evidence for the dimer core is found, and data on the detailed three-body dynamics of the neutral dissociation are also presented for the first time.

2. Experimental

The photoelectron–photofragment coincidence spectrometer employed in these experiments has been described in detail previously, and will only be briefly reviewed here [13]. Ions were created by intersecting a 1 keV electron beam with a 1 kHz pulsed jet expansion of 6% SO₂ seeded in a 30% Ne and 70% He mixture. The anions were extracted and accelerated to 4–6 keV, and subsequently re-referenced to ground by a high-voltage, high-repetition rate potential switch. Anions with m/e of 192 were selected and guided into an interaction region where they were intersected by the third harmonic of a linearly polarized Ti:Sapphire laser (258 nm, 1.2 ps FWHM) which provided a fluence of 1–3 mJ/cm² per pulse.

Photodetached electrons were detected by one of two opposed time- and position-sensitive electron detectors located orthogonal to both the anion and laser beams that collect roughly 20% of the full $4\pi sr$ solid angle. The position information is used to correct for the large Doppler shift induced

by the fast beam and the large collection angle. The photoelectron detectors are calibrated using the photodetachment of I⁻ and have been shown to have resolution of $\sim 5\% \Delta E/E$ at 0.80 eV and 4 keV beam energy.

Neutral fragments recoil out of the fast beam and travel along a 104 cm flight path until they impinge on a set of microchannel plates (MCPs). The charge cloud from the MCPs is detected by a four quadrant time- and position-sensitive delay line anode. Each detector in this array is capable of detecting two particles per dissociation event, as long as they are separated by the 10 ns dead time of the detector electronics. If a perfect anion beam is centered on this detector, conservation of momentum dictates that no more than two particles will hit a given quadrant during a single three-body dissociation event. Conservation of mass and conservation of momentum are used in the CM frame to calculate the mass of each fragment in the dissociation, as detailed previously [14]. Once the masses have been assigned, fragment momenta and energy can be easily calculated. This detector has been shown to have a photofragment energy resolution of roughly $10\% \Delta E/E$ at 0.7 eV, and is calibrated using the photodissociation of O₂⁻.

3. Results

The photoelectron–photofragment correlation spectrum, $N(E_T, eKE)$, for dissociative photodetachment (DPD) of (SO₂)₃⁻ is shown in Fig. 1. Each point in the two-dimensional histogram represents a DPD event with the given correlated photoelectron and photofragment translational energies. The one-dimensional photoelectron and photofragment translational energy spectra are generated by integrating over the conjugate variable in the spectrum. The photoelectron spectrum is consistent with previous studies, peaking at 1.58 eV, yielding a vertical detachment energy (VDE) of 3.22 eV, very close to the 3.20 eV determined by Tsukuda [4]. As in the case of (SO₂)₂⁻, a diagonal structure is observed in the correlation spectrum for (SO₂)₃⁻. The diagonal line in the spectrum represents the maximum translational energy

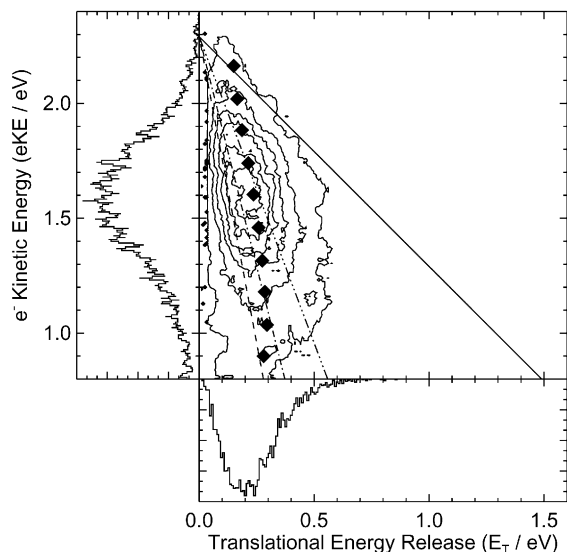


Fig. 1. Photoelectron–photofragment correlation spectrum, $N(E_T, \text{eKE})$, for $(\text{SO}_2)_3^-$ at 258 nm. The uppermost diagonal line represents the maximum translational energy release, KE_{MAX} , for the DPD event. The other three lines represent the expected partitioning into E_T under the impulsive model. The dashed line is for an O–O bond, the dash-dot line is for an S–O bond, and the dash-dot-dot line is for an S–S bond. The filled diamonds represent the average of the E_T distribution at the given eKE.

available to the products, KE_{MAX} , and can be calculated using

$$\begin{aligned} \text{KE}_{\text{MAX}} = & h\nu - D_0((\text{SO}_2)_2^- - (\text{SO}_2)) \\ & - D_0(\text{SO}_2 - \text{SO}_2^-) - \text{EA}(\text{SO}_2) \\ & + E_{\text{INT}}((\text{SO}_2)_3^-), \end{aligned} \quad (1)$$

where $h\nu$ is the photon energy, 4.80 eV, the terms involving D_0 represent the bond dissociation energies for the anion, 1.04 eV for $D_0(\text{SO}_2 - \text{SO}_2^-)$ and 0.36 eV for $D_0((\text{SO}_2)_2^- - (\text{SO}_2))$ [15], and $\text{EA}(\text{SO}_2)$ is 1.11 eV [16]. If the internal energy of the anion is assumed to be negligible due to the use of electron attachment in a free jet expansion as the ion source, $\text{KE}_{\text{MAX}} = 2.29$ eV and matches extremely well with the 5% contour level in Fig. 1. Also shown on the figure are the results of a calculation of the energy partitioning using a soft-bond impulsive model. In this model, soft bonds are assumed between atoms involved in the dissociation and the rest of the molecular framework. Thus,

during dissociation, energy is partitioned based on the relative reduced masses of the two atoms involved and the rest of the molecular framework. The energy partitioned into translation is given by

$$E_T = (\mu_{\text{BC}}/\mu_f)E_{\text{AVL}}, \quad (2)$$

where μ_{BC} is the reduced mass of the two atoms involved in the dissociation and μ_f is the reduced mass of the two larger fragments. The dashed line in Fig. 1 represents the expected E_T for an O–O bond, the dash-dot line for an S–O bond, and the dash-dot-dot line for an S–S bond assuming initial dissociation into $\text{SO}_2 + (\text{SO}_2)_2$. The filled diamonds represent the average E_T at the given eKE.

The molecular-frame differential cross-section (MF-DCS) for the three-body dissociation of $(\text{SO}_2)_3$ is shown in Fig. 2. These types of figures have been used before to investigate the three-body dissociation dynamics of a variety of systems [14,17–20]. They are constructed by first choosing a reference particle for each event. For $(\text{SO}_2)_3$, this reference particle is the fastest photofragment. The velocity of this particle is plotted along the x -axis,

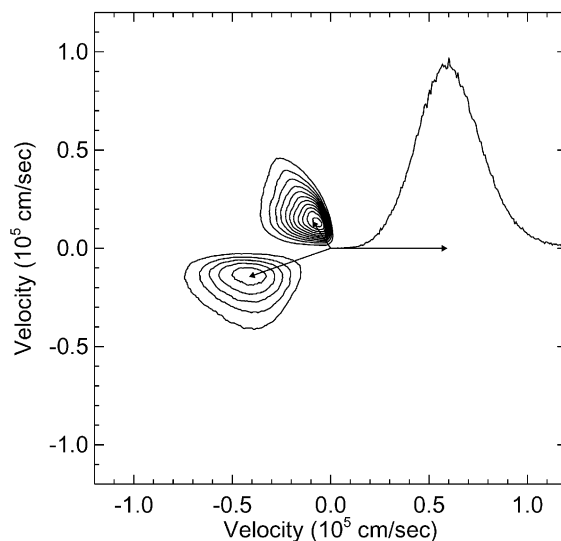


Fig. 2. Molecular-frame differential cross-section for the three-body dissociation of $(\text{SO}_2)_3$. The fastest SO_2 molecule is chosen as the reference particle with a velocity distribution characterized by the line plot. The distributions of the other two SO_2 product velocities are given by the contours as discussed in the text. The arrows are drawn to the centroids of the velocity distributions.

and is shown by the histogram in the upper right hand portion of the plot. For each event, the velocities of the remaining two particles are then rotated into the same plane, and plotted relative to the reference particle. The velocity of the second fastest particle is plotted on the lower half of the plot and the velocity of the slowest particle is plotted on the upper half of the plot. The cutoff of the upper feature at zero velocity results from enforcement of conservation of momentum; given that the reference is the fastest fragment and all fragments have the same mass, no other fragment can have a positive velocity in the x -direction. Arrows are drawn to the centroids of each of the distributions as a visual reference. The spectrum in Fig. 2 shows that two of the particles have roughly equivalent velocities, and the third particle has significantly lower average velocity.

The Dalitz plot, presented in Fig. 3 for DPD of $(\text{SO}_2)_3^-$ is another method for plotting and interpreting momentum distributions among three bodies. For this figure, the plotting method used by Wiese et al. [21] in their study of H_3^+ is employed. A set of coordinates corresponding to the fractional square of the momenta are used. Each axis is given by

$$f(p_i) = p_i^2 / (p_1^2 + p_2^2 + p_3^2), \quad (3)$$

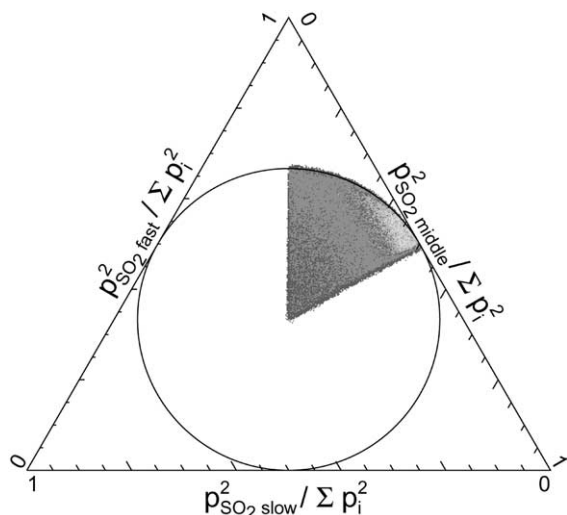


Fig. 3. Dalitz plot representation of the three-body dissociation of $(\text{SO}_2)_3$ showing the partitioning of the fractional square of the momentum among the three particles.

where p_i is the momentum of the i th particle. For a given event, the value of $f(p_i)$ for each particle is plotted as the perpendicular distance from the side of an equilateral triangle. Owing to conservation of energy, all events must lie within the bounds of the triangle. Conservation of momentum constrains all events to lie within the inscribed circle [22]. The relative velocities of each of the photo-fragments is used as a sorting criteria, resulting in all events appearing in 1/6 of the circle in the upper corner of the figure.

4. Discussion

The diagonal feature seen in Fig. 3 was used in the case of $(\text{SO}_2)_2$ to show evidence of the S–O bound dimer [3] in terms of the soft-bond impulse model presented above. A plot of the peak neutral translational energy as a function of the electron kinetic energy revealed that roughly 36% of the available energy was going into translation. According to the impulsive model, this was most consistent with S–O bond fission, where 33% of the available energy would be expected to partition into translation.

The average E_T shown by the diamonds in Fig. 1 does not show close agreement with the predictions of the impulsive model for any of the bond types. At low and high E_T , some deviation is expected from the impulsive model since at low E_T the rest of the molecular framework will have time to respond to the dissociation, breaking the soft-bond assumption, and at high E_T rotation and vibration of the SO_2 products is possible. Additionally, the presence of the third body is likely to cause significant deviation from an impulsive model. Since the third SO_2 is weakly bound to the dimer anion core, it acts neither as part of an SO_2 – SO_2 fragment nor as a completely non-participating third body, making direct application of the impulsive model difficult. Examining the peak of the correlation spectrum, around $E_T = 0.2$ eV and $e\text{KE} = 1.58$ eV, shows closest agreement with either an O–O bond or an S–O bond. Because the deviations from the impulsive model are larger than for the $(\text{SO}_2)_2$ case, it is not possible to assign the bond type to one or the other.

However, the presence of the diagonal feature implies that the trimer system retains much of the character of the dimer system and that the dissociation is somewhat impulsive in nature. The peak positions in the E_T distribution decrease by only 0.02 eV from the dimer to the trimer system. Based on the consistency between the dimer and trimer systems, it can be concluded that the trimer system retains the dimer core, consistent with photoelectron spectroscopy experiments [4] and the energetics of the homogeneous SO_2 cluster anions [5].

The MF-DCS spectrum in Fig. 2 and the Dalitz plot in Fig. 3 are also consistent with the presence of a dissociating dimer core and a spectator SO_2 . In the MF-DCS, the two fastest particles are seen to recoil at nearly 180° with very similar velocities implying that the slowest particle does not participate directly in the dissociation. A very similar MF-DCS was seen for DPD of O_6^- where the partitioning of momentum among the three fragments was even more skewed towards the two fastest fragments [17]. For $(\text{SO}_2)_3$, the broader momentum distribution in the slowest SO_2 fragment is consistent with a larger perturbative effect than in the case of O_6 . Given the greater polarity of the SO_2 fragment, it is not surprising that SO_2 as a third body would perturb a dimer core more than O_2 as a third body. The data were also examined as a function of E_T and the shape of the MF-DCS does not depend significantly on E_T indicating that the shape of the distributions results from variations in the starting geometry as opposed to variations in the dissociation dynamics as a function of E_T .

The energy dependent partitioning of E_T as seen in Fig. 1 implies that the dissociation is fast. Thus, the angular distributions in the MF-DCS should reflect the structure of the anion before photodetachment. Monte Carlo simulations of the three-body dissociation dynamics, to be discussed in detail in a future publication, show a mechanism consistent with a wide range of starting geometries [23]. The distribution of geometries is centered at a symmetrically solvated complex, but the wide distribution causes most dissociation events to occur with significant solvent asymmetry. This is consistent with the momentum distribution of the slowest photofragment in the MF-DCS spectrum,

which is centered near zero x -velocity and has significant angular and velocity variation.

While the MF-DCS is most useful for examining the energy dependence of angular correlations among the fragments, the Dalitz plot is optimal for examining momentum distributions between the three fragments over a wide range of E_T . Most events in the Dalitz plot in Fig. 3 show very little momentum transfer to the slowest fragment. It is interesting to note that although events are concentrated at low momentum transfer to the slow fragment, dissociation events cover the entire accessible area of the plot. Broad distributions in momentum partitioning are consistent with two-step dissociation from a range of starting geometries, since a synchronous mechanism would result in well-defined momentum partitioning. However, the Dalitz plot clearly shows that while a broad distribution of events exist, most dissociations occur with almost no momentum transfer to the slowest fragment. It must be pointed out that a symmetrical linear trimer could also lead to the dissociation dynamics observed here; the two end SO_2 molecules would carry away most of the energy, leaving the central SO_2 molecule nearly stationary. Dynamics of this sort were previously observed in the ionic photodissociation of the linear Ar_3^+ cation [24], however along with previous evidence from photoelectron and absorption spectroscopies [4,5], we take the observed dynamics as evidence for the dimer core.

5. Conclusions

The dissociative photodetachment dynamics of $(\text{SO}_2)_3^-$ were studied using photoelectron–photofragment coincidence spectroscopy. In agreement with previous studies, evidence was found for a dimer-like core in the trimer system. The photoelectron–photofragment correlation spectrum revealed a diagonal feature that was interpreted in terms of a soft-bond impulsive model, consistent with either O–O or S–O bonding in the dimer core of $(\text{SO}_2)_3^-$, although the loosely bound nature of the third SO_2 molecule reduces the ability of the impulsive model to be applied to the dissociation. The three-body dissociation dynamics of neutral

(SO₂)₃ are also consistent with the presence of a dimer core. The slowest SO₂ fragment in each dissociation event received only a very small portion of the translational energy release, acting almost as a spectator. The dynamics are consistent with photodetachment from a wide range of geometries indicating that the position of the third SO₂ molecule is not well-defined in the cluster. The two SO₂ fragments from the dimer core, on the other hand, recoil at nearly 180° in the center of mass frame. Previous spectroscopic data [4,5] combined with the lack of significant momentum transfer to the third SO₂ fragment and the nearly identical translational energy release as in the dimer system gives strong evidence for dissociation of a dimer core with a solvating SO₂ spectator.

Acknowledgements

This work was supported by the Air Force Office of Scientific Research (AFOSR) under Grant F49620-000-10-010.

References

- [1] J.V. Coe, Chem. Phys. Lett. 229 (1994) 161.
- [2] R.V. Hodges, J.A. Vanderhoff, J. Chem. Phys. 72 (1980) 3517.
- [3] R.-J. Li, L.N.S. Alconcel, R.E. Continetti, Chem. Phys. Lett. 336 (2001) 81.
- [4] T. Tsukuda, T. Hirose, T. Nagata, Int. J. Mass Spectrom. Ion Process. 171 (1997) 273.
- [5] T. Dresch, H. Kramer, Y. Thurner, R. Weber, Z. Phys. D 18 (1991) 391.
- [6] T. Dresch, H. Kramer, Y. Thurner, R. Weber, Chem. Phys. Lett. 177 (1991) 383.
- [7] J.T. Snodgrass, J.V. Coe, C.B. Freidhoff, K.M. McHugh, K.H. Bowen, J. Chem. Phys. 88 (1988) 8014.
- [8] H.-S. Kim, M.T. Bowers, J. Chem. Phys. 85 (1986) 2718.
- [9] N. Berthe-Gaujac, I. Demachy, Y. Jean, F. Volatron, Chem. Phys. Lett. 221 (1994) 145.
- [10] N. Berthe-Gaujac, Y. Jean, F. Volatron, Chem. Phys. Lett. 243 (1995) 165.
- [11] M. Iraqi, N. Goldberg, H. Schwarz, Int. J. Mass Spectrom. Ion Process. 130 (1994) 127.
- [12] R.E. Continetti, Int. Rev. Phys. Chem. 17 (1998) 227.
- [13] K.A. Hanold, A.K. Luong, T.G. Clements, R.E. Continetti, Rev. Sci. Instrum. 70 (1999) 2268.
- [14] A.K. Luong, T.G. Clements, R.E. Continetti, J. Phys. Chem. A 103 (1999) 10237.
- [15] J.R. Vacher, M. Jorda, E. Le Duc, M. Fitaire, Int. J. Mass Spectrom. Ion Process. 114 (1992) 149.
- [16] M.R. Nimlos, G.B. Ellison, J. Phys. Chem. 90 (1986) 2574.
- [17] A.K. Luong, T.G. Clements, R.E. Continetti, in: A.G. Suits, R.E. Continetti (Eds.), Imaging in Chemical Dynamics, American Chemical Society, Washington, DC, 2001, p. 312.
- [18] T.G. Clements, A.K. Luong, H.-J. Deyerl, R.E. Continetti, J. Chem. Phys. 114 (2001) 8436.
- [19] S. Hsieh, J.H.D. Eland B, J. Phys. At. Mol. Opt. Phys. 30 (1997) 4515.
- [20] M. Lavollée, V. Brems, J. Chem. Phys. 110 (1999) 918.
- [21] L.M. Wiese, O. Yenen, B. Thaden, D.H. Jaacks, Phys. Rev. Lett. 79 (1997) 4982.
- [22] R. Hagedorn, Relativistic Kinematics; a Guide to the Kinematic Problems of High-Energy Physics, W.A. Benjamin, New York, 1963.
- [23] T.G. Clements, R.E. Continetti, in preparation.
- [24] J.T. Snodgrass, C.M. Roehl, M.T. Bowers, Chem. Phys. Lett. 159 (1989) 10.